Beyond Lattice Models of Activated Transport in Zeolites: High-Temperature Molecular Dynamics of Self-Diffusion and Cooperative Diffusion of Benzene in NaX

Harikrishnan Ramanan,[†,‡] Scott M. Auerbach,*[,†,§] and Michael Tsapatsis[†,‡]

Departments of Chemical Engineering and of Chemistry, University of Massachusetts, Amherst, Massachusetts 01003, and Department of Chemical Engineering and Materials Science, University of Minnesota, Minneapolis, Minnesota 55455

Received: June 2, 2004; In Final Form: August 11, 2004

We employ high-temperature molecular dynamics to investigate self-transport and cooperative transport of benzene in NaX (Si:Al = 1.2). We have refined the benzene−NaX force field for use with our previously developed framework force field for aluminosilicates, which explicitly distinguishes between Si and Al atoms in the frame, and also between oxygen atoms in Si−O−Si and Si−O−Al environments. Energy minimizations and molecular dynamics simulations performed to test the new force field give excellent agreement with experimental data on benzene heats of adsorption, benzene−Na distances, and Na distributions for benzene in NaY (Si:Al = 2.4) and NaX (Si:Al = 1.2). Molecular dynamics simulations are performed over a range of temperatures (600−1500 K) and loadings (infinite dilution to four benzenes per supercage) to evaluate simultaneously the self-diffusivities and cooperative (alternatively Maxwell−Stefan) diffusivities. The simulated diffusivities agree well with pulsed field-gradient NMR and quasi-elastic neutron scattering data. Despite this agreement, we show in the following companion paper that membrane fluxes calculated with our diffusivities overestimate experiments by 1 order of magnitude when support resistance is accounted for in the transport model, and by about 2 orders of magnitude when support resistance is neglected. This discrepancy may arise from the polycrystalline nature of present-day NaX membranes.

I. Introduction

Zeolites offer useful properties such as highly selective adsorption, diffusion, and reaction;[1] although their small pore sizes and complex transport pathways provide significant resistances to molecular motion.[1−3] Computational studies can elucidate the mechanisms of transport, thereby helping to optimize the balance between high selectivity and high flux.[4−9] Such studies are especially timely given the importance of zeolite membranes, which promise novel applications but suffer from structural disorder.[10] In the present article we apply high-temperature molecular dynamics (MD) to elucidate the temperature and loading dependencies of self-diffusion and cooperative diffusion of benzene in NaX zeolite. In the companion article that follows, we use these diffusivities to estimate benzene fluxes through NaX membranes, for comparison with permeation measurements.

Significant effort has been devoted to understanding benzene adsorption and diffusion in NaX and NaY, because of persistent, qualitative discrepancies between different experimental probes of the loading dependence of self-diffusion.[11] Pulsed field-gradient (PFG) NMR self-diffusivities for benzene in NaX decrease monotonically with loading,[12] whereas tracer zero-length column (TZLC) data *increase* monotonically with loading.[11] This discrepancy casts doubt on using experimental diffusivities for designing processes in zeolites. In previous work, we have endeavored to shed light on this problem by simulating the loading dependence of benzene self-diffusion in NaX as accurately as possible. This task is challenging because (i) benzene diffusion is dominated by rare site-to-site jumps, which are most efficiently captured by lattice models, and (ii) benzene−benzene attractions, which are relatively strong, are most conveniently treated by off-lattice models. We thus set out to develop a realistic lattice model of benzene in NaX with guest−guest attractions,[13] parametrized by accurate transition state theory calculations.[14] Our previous lattice model results were found to be in excellent qualitative agreement with PFG NMR, and in qualitative disagreement with TZLC.[15]

Although such lattice models are conceptually illustrative, they often require approximations that one would eventually like to relax. In particular, one often assumes (i) a temperature- and loading-independent lattice of sites, (ii) no influence from cation dynamics, and (iii) an approximate treatment of guest−guest interactions. In the present work, we relax these assumptions by performing high-temperature MD. High temperatures provide enough thermal energy to surmount relatively large barriers, whereas MD provides a natural treatment of guest−guest interactions. The disadvantage of this approach is that temperatures relevant to membrane permeation measurements are usually much lower than those required for simulating diffusive motion in cation-containing zeolites. Extrapolating diffusivities to lower temperatures assuming an Arrhenius temperature dependence is valid if the basic mechanism for diffusion does not change from high to low temperature. At lower temperatures we surmise that benzene makes rare jumps among supercage Na cations. At higher temperatures, it is possible that cooperative benzene−Na motions may become activated. In the present article, we explore whether such cooperative motions are important for benzene in NaX, and

* Address correspondence to this author. E-mail: auerbach@chem.umass.edu.

† Department of Chemical Engineering, University of Massachusetts.

‡ Department of Chemical Engineering and Materials Science, University of Minnesota.

§ Department of Chemistry, University of Massachusetts.

10.1021/jp0476242 CCC: $27.50 © 2004 American Chemical Society
Published on Web 10/13/2004

hence whether high-temperature MD can be used to simulate accurate diffusivities in cation-containing zeolites.

To address such issues, a force field that provides a faithful representation of cation locations and motions must be used. We have previously reported such a force field, which explicitly distinguishes Si and Al atoms in the frame, and also between oxygen atoms in Si−O−Si and Si−O−Al environments.[16] In the present article, we report a refined benzene−NaX force field for use with the explicit aluminosilicate framework force field. Although all these improvements are welcomed, they also present a conceptual problem. In particular, relative to our previous simulations of benzene self-diffusion in NaX, we improve both the force field and the dynamics in the present article. That makes comparison with old results ambiguous, because we do not know whether discrepancies arise from the improved potential or dynamics. It would be optimal to run high-temperature MD using both the old and new force fields, to disentangle the effects of improving both the force field and the dynamics. However, calculating statistically converged diffusivities with the new force field already sequestered our computational resources. This is especially true for the Maxwell−Stefan diffusivities, which are crucial for calculating membrane fluxes (see following paper for details), but which are difficult to converge because they probe cooperative motions of the adsorbed phase. In future work, we plan to complete this stepwise improvement by running high-temperature MD using the old force field model.[14,17,18] Nonetheless, the present work represents perhaps the most accurate simulations to date of hydrocarbon motion in cation-containing zeolites, which we utilize in the companion paper that follows for computing benzene fluxes through NaX membranes.

Below we show that our MD simulations produce diffusivities in excellent agreement with microscopic measurement techniques such as PFG NMR and quasi-elastic neutron scattering (QENS).[1] On the other hand, in the companion paper we find that membrane fluxes obtained from our simulated diffusivities overestimate experimental values, a discrepancy reminiscent of that between PFG NMR and TZLC noted above. Vasenkov et al. recently reported PFG NMR self-diffusivities that depend on the length scale probed,[19] demonstrating that zeolites may not be as ordered as we surmise them to be. Instead, they may suffer from subtle patterns of disorder that impact transport in measurable ways. Such disorder may lie at the heart of discrepancies between simulated and measured fluxes through zeolite membranes.

The remainder of this article is organized as follows: section II describes the simulation methods, section III gives results and discussion, and in section IV we summarize and give concluding remarks.

II. Methods

In this section, we describe the systems simulated, and the force fields employed to carry out the simulations, including the optimization of the new benzene−NaX force field. We also detail the molecular dynamics calculations, and how we use these to compute self-diffusivities and Maxwell−Stefan diffusivities.

A. System. The FAU pore topology consists of sodalite cages (also called β cages) connected by double six-membered-rings (6MR), each with six tetrahedral atoms (Si or Al) and with a free aperture diameter of ca. 0.22 nm. This creates a large cavity or supercage with four tetrahedrally located 12MR pore openings (free aperture diameter of ca. 0.74 nm) and a three-dimensional channel system (Figure 1). The FAU unit cell has cubic symmetry and consists of eight supercages and eight sodalite cages.[20] The number of cations in the system depends on the Si:Al ratio, as each Al atom brings in a negative charge to be compensated by an extraframework Na cation. In this work, we have simulated two FAU-type zeolites: (i) NaY: Si:Al = 2.43, 56 Na cations per unit cell, *Fd*3*m* (cubic) symmetry, lattice parameter $a = 24.85$ Å; and (ii) NaX: Si:Al = 1.23, 86 cations per unit cell, *Fd*3 (cubic) symmetry, $a = 25.099$ Å.[27,28]

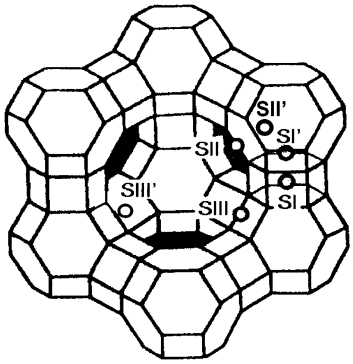

Figure 1. Framework structure of FAU with different cation types.

B. Force Field. The force field used in the present study is based on the explicit T-atom model developed by Jaramillo and Auerbach for modeling Na cation motion in aluminosilicates.[16] This choice was made to allow for a faithful representation of Na−benzene motions, should such motions become important at higher temperatures. The explicit T-atom model provides the flexibility to generate force fields for systems with widely different Si:Al ratios, by distinguishing between Si and Al in the framework as well as oxygen atoms in Si−O−Si and Si−O−Al environments.

The intramolecular guest (benzene) potential is taken from our earlier work on benzene in NaX and NaY.[17] Guest−guest interactions are represented by Coulombic and Lennard-Jones potentials according to

$$V_{BB} = V_{Coulombic} + V_{LJ} = \sum_{cells}\sum_{j\in B}\sum_{i\in B}\frac{q_i q_j}{r_{ij}} + \sum_{j\in B}\sum_{i\in B} 4\epsilon_{ij}\left[\left(\frac{\sigma_{ij}}{r_{ij}}\right)^{12} - \left(\frac{\sigma_{ij}}{r_{ij}}\right)^{6}\right] \quad (1)$$

where i and j refer to atoms belonging to different benzene molecules. The guest−guest Coulombic energy is evaluated using Ewald sums. The intermolecular interaction parameters for benzene are chosen from Catlow et al.[21]

Perhaps the most important part of the force field is the host−guest (NaX−benzene) contribution, which needs to be re-optimized for use with the explicit T-atom model. We perform re-optimization using energy minimization methods,[16,17] for comparison with experimental benzene adsorption heats. Although adsorption heats are measured at finite temperatures, whereas energy minimization corresponds to zero temperature, we perform such minimizations because they are typically faster than finite-temperature simulations. Such computational speed is particularly important when a new potential is optimized, which requires many calculations for different potential parameters.

We estimate finite-temperature adsorption enthalpies from energy minimizations using harmonic-oscillator and ideal-gas approximations. To see how, we begin with the molar adsorption energy, given by $\Delta U_{ads} = \langle V(zg)\rangle - [\langle V(z)\rangle + \langle V(g)\rangle]$, where $\langle V(zg)\rangle$, $\langle V(z)\rangle$, and $\langle V(g)\rangle$ are the average potential energies of zeolite+guest, bare zeolite, and isolated guest, respectively, all

TABLE 1: Optimized Lennard-Jones 6-12 Model Parameters for Benzene−FAU Interactions

atom pair type	σ (Å)	ϵ (eV)
O_s−C	3.007	7.67×10^{-3}
O_a−C	3.007	7.67×10^{-3}
O_s−H	2.606	6.139×10^{-3}
O_a−H	2.606	6.139×10^{-3}
Na−C	3.545	1.324×10^{-3}
Na−H	2.944	1.255×10^{-3}

averaged in the canonical ensemble at temperature T. Assuming that the zeolite+guest, bare zeolite and isolated guest are all classical harmonic oscillators,[22] the molar adsorption energy becomes $\Delta U_{ads}\ V_0(zg) - [V_0(z) + V_0(g)] + 3RT$, where $V_0(zg)$, $V_0(z)$, and $V_0(g)$ are the respective minimum potential energies, and R is the gas constant. This result is obtained because (i) the canonical average of each harmonic mode is $3RT/2$, independent of frequency, and (ii) the six free translation/rotation modes in the gas phase are presumed to become vibrations in the adsorbed phase, yielding a net thermal energy of $3RT$. The adsorption enthalpy is given by $\Delta H_{ads} = \Delta U_{ads} + \Delta pV = \Delta U_{ads} + p\Delta V = \Delta U_{ads} + p(V_{ads} - V_{gas}) \approx \Delta U_{ads} - pV_{gas} \approx \Delta U_{ads} - RT$. The second equality arises from assuming adsorption at constant pressure; the first approximation ignores the adsorbed-phase volume compared to the gas-phase volume, and the final approximation assumes the ideal-gas equation of state for the gas. Putting these results together yields: $\Delta H_{ads} \approx V_0(zg) - [V_0(z) + V_0(g)] + 2RT$. The experimentally reported heat is just $-\Delta H_{ads}$.

In practice, $V_0(g) = 0$ with our valence-bond force field for benzene; $V_0(z)$ is calculated once only because it is independent of the updated host−guest potential. The quantity $V_0(zg)$ is thus the main result from host−guest energy minimization. Using the MD-DOCKER module of the DIZZY program,[23] a minimum of 150 independent energy minimizations are first performed on the bare zeolites NaX and NaY, keeping the framework atoms fixed and allowing the cations to obtain the most stable distributions. A typical minimization run consists of at least 1000 MD steps at 1000 K, followed by system cooling using the dynamic minimization algorithm developed by Snyman.[24−26] Minimizations are then performed for a benzene loading of eight molecules per unit cell, i.e., an average of one benzene per supercage of NaX and NaY. These minimizations are performed without guest−guest interactions, to enhance the efficiency of sampling minimum-energy sites at infinite dilution. Host−guest Lennard-Jones interaction parameters are adjusted to fit (a) experimentally observed heats of sorption and (b) zeolite−guest binding locations measured by powder neutron diffraction studies on benzene in NaX and NaY.[27,28]

C. Molecular Dynamics. We performed molecular dynamics in the *NVE* ensemble using periodic boundary conditions for benzene in NaX.[29] Keeping the framework atoms fixed and allowing the cations and benzene molecules to move, the system is equilibrated for about 100 ps and dynamics continued for about 0.5−5 ns at $T = 600-1500$ K using 1 fs time steps to generate equilibrium data. The center of mass (COM) locations of benzene are stored every 5−10 fs, whereas cation locations are stored every 50 fs. The system temperature and energies are reported every 25 fs to check the stability of the molecular dynamics runs, and to evaluate useful thermodynamic properties.

As discussed above, we allow for cation motion alongside benzene motion in our MD simulations. On the basis of experimental observations, the motion of cations in zeolites is understood to be based on two mechanisms: (a) migration of cations from site to site (highly correlated cation motion) and (b) restricted or local cation motion (cation relaxation).[30] The observed activation energy for Na ion relaxation in NaX (30 kJ/mol)[31] is considerably lower than that reported for ionic conduction or migration (52.3−56.8 kJ/mol).[30] Studies based on magic angle spinning NMR spectroscopy and dielectric spectroscopy[30,32−34] show a wide range of activation energies

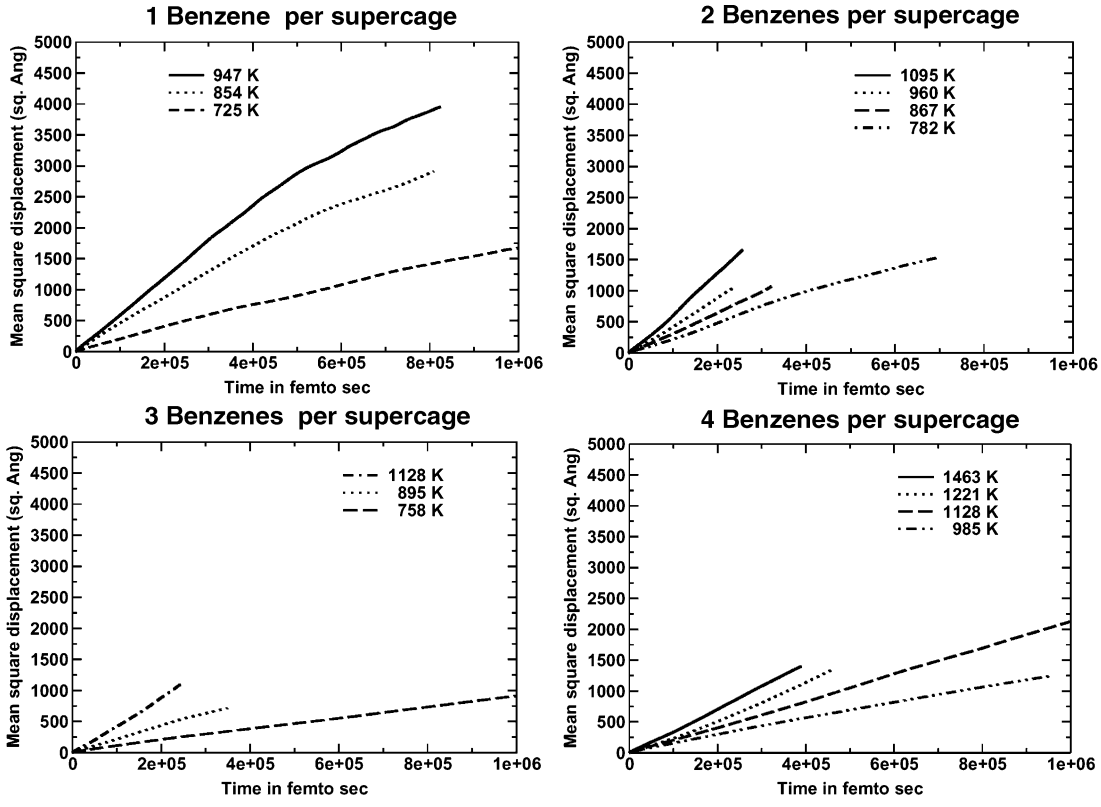

Figure 2. Mean-square displacement charts for the self-diffusivities of benzene in NaX.

TABLE 2: Summary of Sorption Energies and Cation Occupancies for Minimized Configurations of Benzenein NaY and NaX (Infinite Dilution Loading)

	NaY		NaX	
criterion	simulation	experiment	simulation	experiment
Heat of adsorption (kJ/mol @ 323 K)	80.4 ± 2.49	79.5 ± 0.7[42] 78[54,55]	84.3 ± 2.97	83.5 ± 0.7[42] 73[54,55]
d_{COM}-Na[c] (Å)				
Site II cation	2.72 ± 0.015[a]	2.70[27]	2.72[b]	2.70[27]
Site III cation	2.72[a]		2.68 ± 0.033	2.72[28,43]

[a] Out of eight benzenes in a NaY unit cell, seven were located near the SII cations and one near the SIII cation. [b] Out of eight benzenes in a NaX unit cell, one was located near the SII cations, five near the SIII cations, and two near SIII′. [c] Distance of benzene center-of-mass to Na cation.

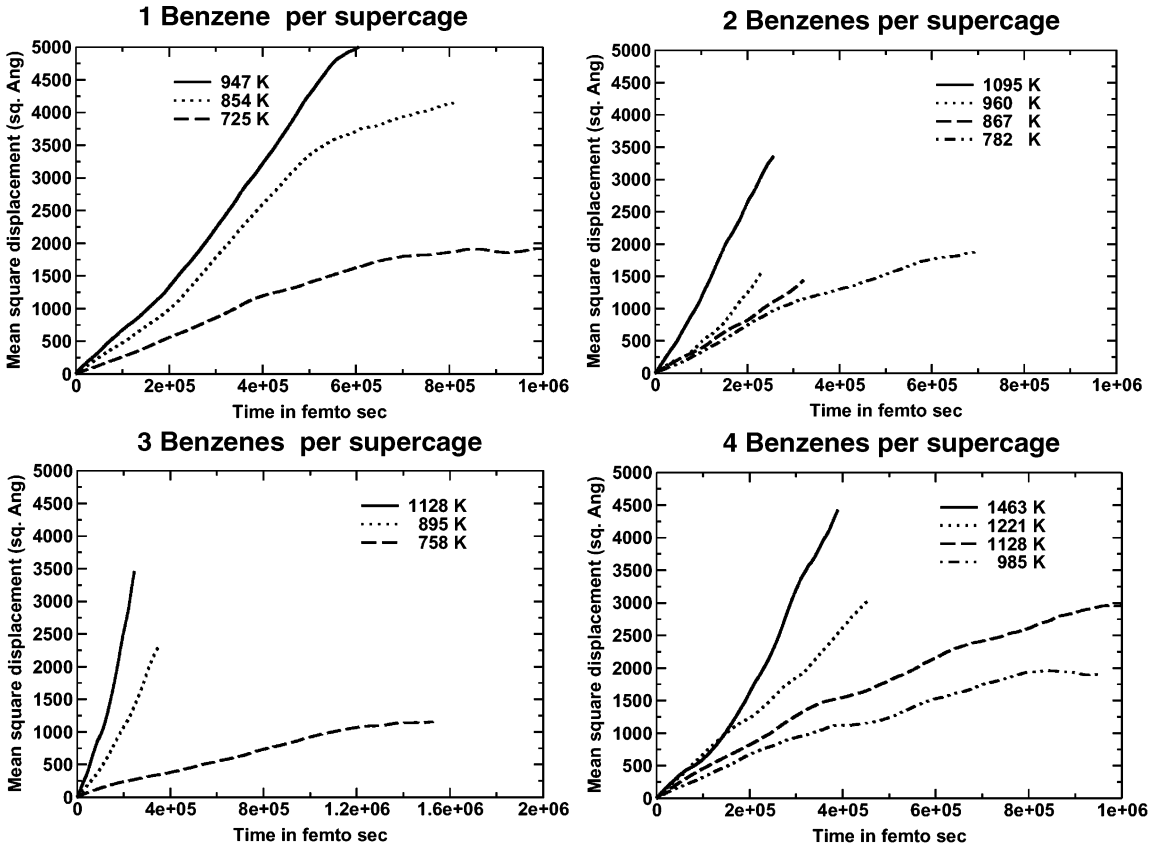

Figure 3. Mean-square displacement charts for the Maxwell−Stefan diffusivities of benzene in NaX.

for cation motion in zeolites, e.g., an activation energy of E_{act}(Li) = 13 kJ/mol for Li motion in dehydrated LSX zeolite[34] to E_{act}(Cs) = 109 kJ/mol for Cs in analcite.[33] Considering the range of activation energies observed for cation motion in zeolites, we allowed the cations to move during the dynamics of benzene to determine if Na cations diffuse alongside benzenes, or whether cations remain localized at sites. Cation dynamics also serve as an effective heat bath for the system, because of the strong coupling among cations and benzenes. We checked the effectiveness of this heat bath by computing the relative-root-mean-square temperature fluctuations, $T/\langle T\rangle$, during MD simulations. Typical values are found to be 0.06 for temperatures around 1000 K, thus confirming that the statistics of the canonical ensemble are captured during the simulations.

Minimum-energy configurations were generated using the minimization procedure discussed above. Dynamics runs were initiated from such configurations at different temperatures (600−1500 K) and benzene loadings (infinite dilution to four benzenes per supercage). The simulations were performed at high temperatures to produce reliable estimates for the mean-square displacements of benzene molecules for the whole range of loading conditions.

D. Dynamical Information Derived from MD: The random motion of benzene diffusion is characterized by the self-diffusion coefficient D_s, and the Maxwell−Stefan diffusion coefficient D^{MS}.[35,36] These diffusivities are computed from mean-square displacements (MSD) using the Einstein relations according to[1,4,37]

$$D_s = \lim_{\Delta t\to\infty} \frac{1}{6(\Delta t)} \frac{1}{N} \left\langle \left[\sum_{k=1}^{N} |\vec{r}_k(t+\Delta t) - \vec{r}_k(t)|^2 \right] \right\rangle \qquad (2)$$

$$D^{MS} = \lim_{\Delta t\to\infty} \frac{1}{6(\Delta t)} \frac{1}{N} \left\langle \left[\sum_{k=1}^{N} \sum_{l=1}^{N} (\vec{r}_k(t+\Delta t) - \vec{r}_k(t))(\vec{r}_l(t+\Delta t) - \vec{r}_l(t)) \right] \right\rangle \qquad (3)$$

where $\vec{r}_l(t)$ is the three-dimensional sorbate position at time t and N is the component loading. Under conditions when correlations between different molecules are unlikely, it can be easily seen from eqs 2 and 3 that $D^{MS} = D_s$. Equation 2 shows that self-diffusion is a property of an individual, tagged diffusant, whereas eq 3 shows that the Maxwell−Stefan diffusivity reflects

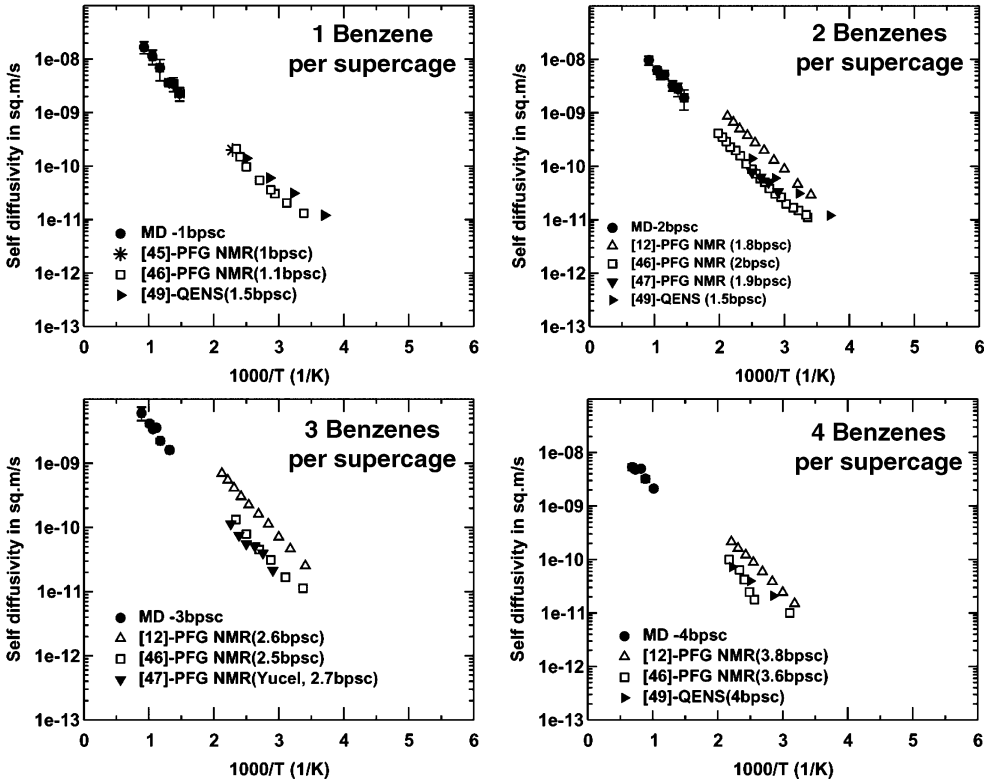

Figure 4. Arrhenius temperature dependence of the self-diffusivities of benzene in NaX. Error bars shown for our MD results are occasionally found to be smaller than the size of the legend symbols used.

a cooperative transport property of all diffusants in the system. This makes converging the self-diffusion coefficient easier because each guest contributes its own set of statistics, whereas, in Maxwell−Stefan diffusion there is only one set of statistics regardless of loading. To enhance convergence, and to provide straightforward error bars, we performed three independent runs for each value of loading and temperature.[38,39] The standard deviation in the temperature for each MD run is estimated from the average fluctuation about the mean T along the whole length of the simulation. The standard deviation in the diffusivity is estimated from averaging the results from the three identical MD runs performed from different starting configurations of the benzene−NaX system. With the above error bars in the temperature and diffusivity, the error bars in the activation energies and Arrhenius preexponential factors are determined using the statistical analysis program,[40] which incorporates the error in both temperature and diffusivity while the average slope (related to activation energy) and intercept (related to preexponential factor or site-to-site jump frequency) and their respective standard deviations are estimated.

To evaluate diffusion coefficients representative of long-range motion, mean-square displacements are consistently sampled in the range 500 Å^2 ≤ MSD ≤ 1500−3000 Å^2, which corresponds to observation lengths at least as large as the simulation box. Sampling the entire simulation cell, and not just cage-to-cage length scales, is important when an explicit Si/Al framework model is used. This is because electrostatic disorder in the framework can lead to electrostatic traps[41] that all molecules need to sample.

To summarize, we generate statistics for single-molecule and cooperative motion (for self-diffusivities and Maxwell−Stefan diffusivities, respectively) through MD simulations at various temperatures and loadings. Below we present the results for the transport coefficients of benzene in NaX, $D_s(T,\Theta)$ and $D^{MS}(T,\Theta)$, and the respective activation energies, $E_{act}^{s}(\Theta)$ and $E_{act}^{MS}(\Theta)$.

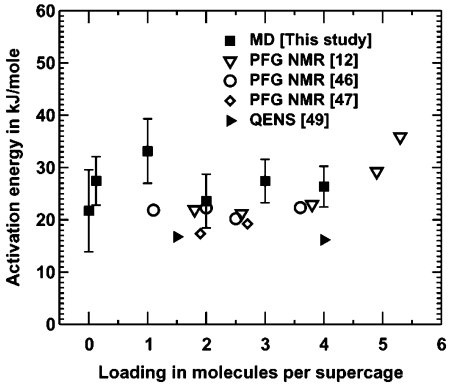

Figure 5. Loading dependence of the energy of activation for self-diffusion of benzene in NaX.

III. Results and Discussion

In this section, we discuss the re-optimized host−guest potential, the cation dynamics, and the diffusion dynamics of benzene in NaX.

A. Re-optimized Host−Guest Potential. We performed energy minimizations on NaY (Si:Al = 2.42) and NaX (Si:Al = 1.23) with a loading of one benzene per supercage without guest−guest interactions (see section IIB), adjusting host−guest Lennard-Jones 6-12 parameters to fit experimental adsorption heats and guest binding configurations. The Lennard-Jones 6-12 parameters for the benzene−zeolite interactions for the newly optimized potential are listed in Table 1. The binding energies estimated from our force field show excellent agreement with the experimental heats of sorption for benzene in NaY and NaX reported by Dzhigit and co-workers[42] (Table 2). In addition, as shown in Table 2, the estimated benzene−cation distances (averaged over all benzenes at the specific cation site) at the SII site for NaY, and the SII and SIII sites for NaX, are in excellent agreement with experimental neutron diffraction

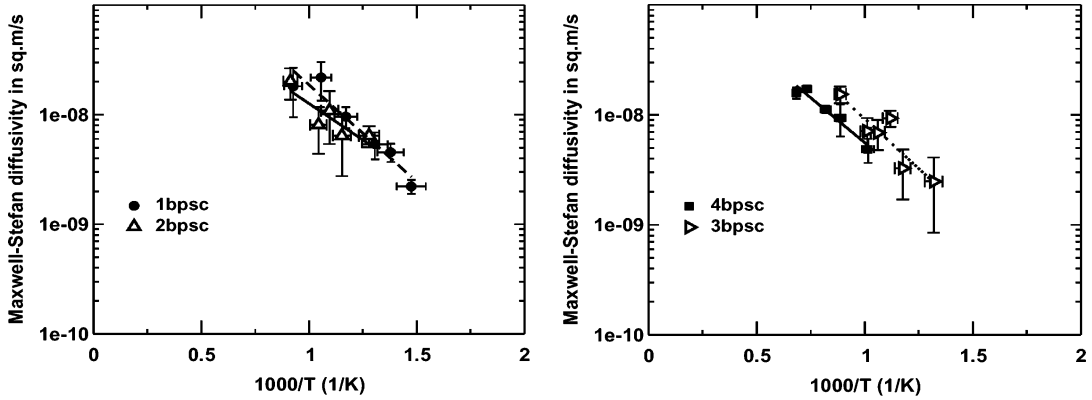

Figure 6. Temperature dependence of the Maxwell−Stefan diffusivities of benzene in NaX. Error bars shown for our MD results are occasionally found to be smaller than the size of the legend symbols used.

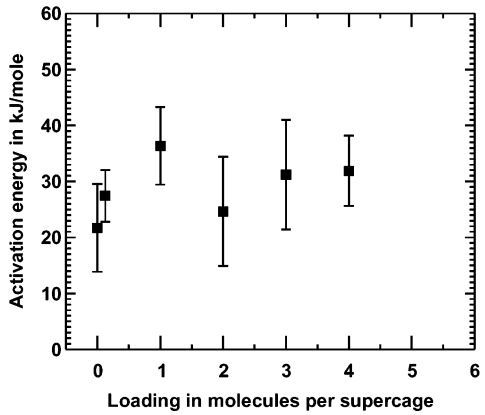

Figure 7. Loading dependence of the energy of activation for Maxwell−Stefan diffusion of benzene in NaX.

data.[27,28,43,44] Consistent with powder neutron diffraction studies for NaY[27] and NaX,[28,43] we found benzene to be located predominantly near SII cation sites for NaY, and near SII, SIII and SIII′ cation sites for NaX.

B. Dynamics of Cation Motion. The mean-square displacements of representative cations initially located at sites I, I′, II, II′, III, and III′ (see Figure 1) are analyzed for temperatures in the range 578−1067 K during dynamics at infinite benzene dilution. Only in-site vibrations are observed for cations at sites I, I′, and II′ for all temperatures studied; their mean-square displacements are found to be on the order of 1 Å^2. Most site II cations were found to exhibit similar sluggish motion, though a few showed displacements on the order of 10 Å^2, with an activation energy of E_{act}(Na,II) = 42 kJ/mol. For the case of site III and III′ cations, we observed mean-square displacements on the order of 50−150 Å^2 for temperatures in the 850−1100 K range, giving activation energies in the range E_{act}(Na,III/III′) = 36−46 kJ/mol. Thus, even at elevated temperatures, our simulations suggest that cation motion is localized at sites or within supercages, in contrast to guest motion, which spans many cages over comparable time scales (see below). These results lend credence to our overall approach of using high-temperature MD to extract low-temperature diffusivities in cation-containing zeolites.

C. Diffusion of Benzene in NaX. Figures 2 and 3 show the individual tagged molecule mean-square displacements (MSDs) for self-diffusion and the collective MSDs for Maxwell−Stefan diffusion, respectively, for various temperatures in the range 725−1463 K, and benzene loadings (Θ = 1−4 molecules per supercage). The superior statistics obtained for self-diffusion is exhibited in the generally better linearity of long-time MSDs in Figure 2, as compared with that in Figure 3. In all cases, diffusivities were extracted from MSD slopes in the range 500 Å^2 ≤ MSD ≤ 1500−3000 Å^2. Final diffusivities were obtained by averaging over three distinct runs, with the same loading and approximate temperature.

In Figure 4, we compare the estimated temperature dependence of benzene's self-diffusivity in NaX with experimental data from pulsed field-gradient NMR (PFG-NMR)[12,45−47] and quasi-elastic neutron scattering (QENS).[48,49] As expected for a guest−zeolite system where guest motion is dominated by jump diffusion, the self-diffusivity obeys the Arrhenius temperature dependence. Extrapolating our high-temperature MD diffusivities to the experimentally probed temperatures gives excellent agreement in both the order of magnitude and activation energies of diffusion.

Figure 5 shows the estimated loading-dependent activation energies, $E^s_{act}(\Theta)$, for comparison with data from PFG-NMR and QENS experiments. From our MD simulations, the mean value of $E^s_{act}(\Theta)$ shows a sharp increase from 22 kJ/mol (Θ = 0, infinite dilution) to 33 kJ/mol (Θ = 1), followed by a decrease to ∼24 kJ/mol at Θ = 2 and an approximately constant value of ∼27 kJ/mol for higher benzene loadings Θ = 3, 4. However, due to the significant overlap between the error-bars, $E^s_{act}(\Theta)$ could also be interpreted as being independent of loading. Nevertheless, the order of magnitude of the MD-simulated activation energies is reasonably close to the experimental data. Our simulations overestimate PFG-NMR results[46] for Θ = 1 and QENS data[49] at Θ = 1.5, 4. Considering the range of loadings investigated, such remarkable agreement between our MD simulations and experiment is very encouraging.

In Figure 6, we show the temperature dependence of Maxwell−Stefan diffusivities for benzene in NaX. These also exhibit Arrhenius temperature dependence, though with activation energies different from self-diffusion values. Figure 7 shows the loading dependence of the activation energy for Maxwell−Stefan diffusion of benzene in NaX. As observed for the self-diffusion process, we obtain a strange trend for $E^{MS}_{act}(\Theta)$, for which a simple interpretation is not obvious to us at present. Nevertheless, the similarity in the trends shown by $E^s_{act}(\Theta)$ and $E^{MS}_{act}(\Theta)$ may follow from the equivalence in the underlying jump-diffusion mechanism controlling both self-diffusion and Maxwell−Stefan diffusion.

In Figure 8A,B, we compare the loading dependencies of the MD-simulated self-diffusivities and Maxwell−Stefan diffusivities for benzene in NaX at temperatures in the range 755−1094 K. We observe in Figure 8A that the self-diffusivities decrease with loading, consistent with a picture of jump diffusion with site blocking. In Figure 8B, we see that the Maxwell−Stefan

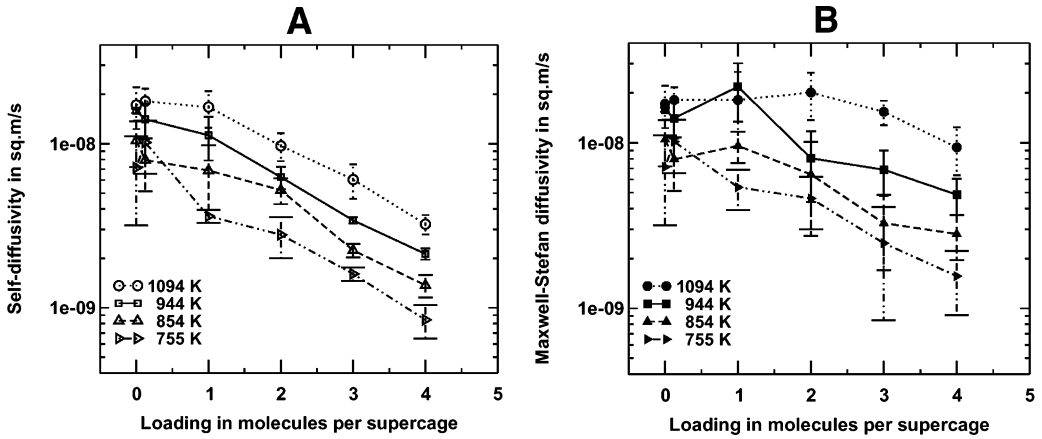

Figure 8. Isotherms representing loading dependencies of the (A) self-diffusivities and (B) Maxwell−Stefan diffusivities of benzene in NaX. Lines connecting points are shown to guide through discussion in text. Error bars shown for our MD results are occasionally found to be smaller than the size of the legend symbols used.

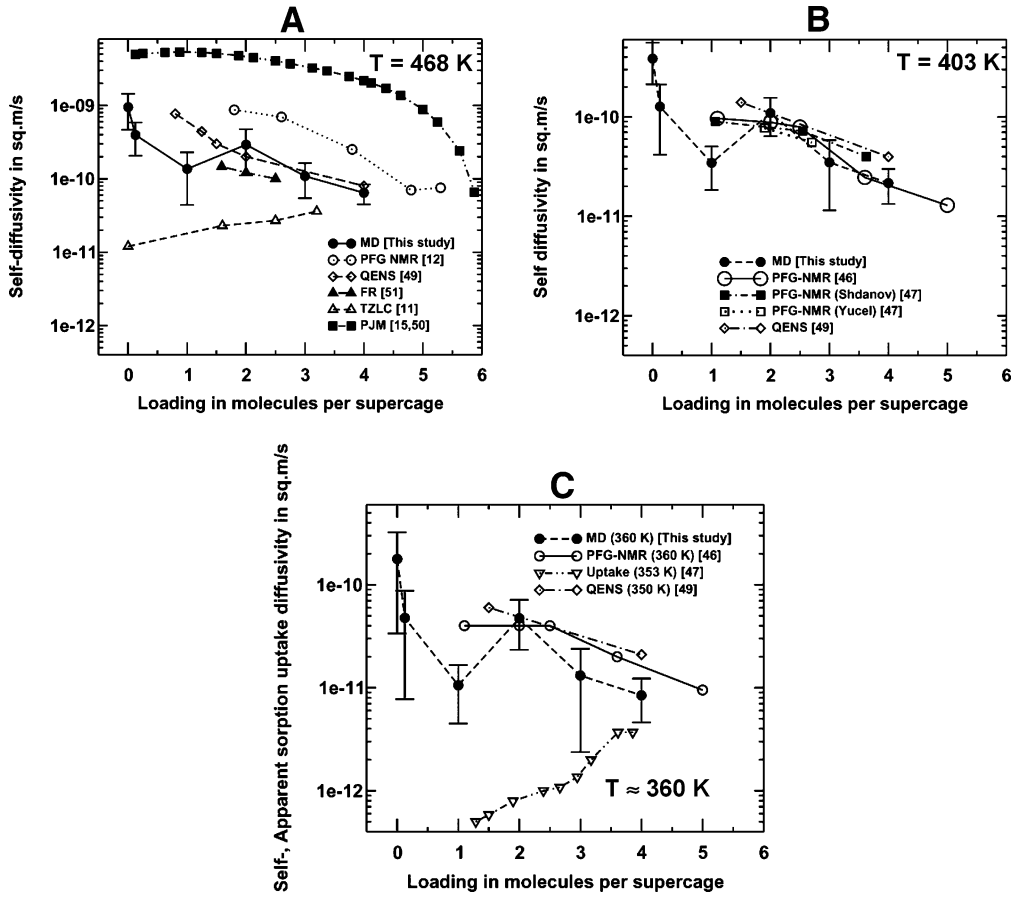

Figure 9. Comparison of diffusion isotherms extrapolated from high-temperature MD simulations with experimental diffusion isotherms of benzene in NaX at (A) 468 K, (B) 403 K, and (C) ∼360 K. Lines connecting points are shown to guide through discussion in text.

diffusivities do not decrease as strongly as the self-diffusivities. This is consistent with the notion that Maxwell−Stefan diffusion is less susceptible to vacancy effects than is self-diffusion.[1,37] Figure 8B suggests that an increasing loading dependence at low loadings may be present for the Maxwell−Stefan diffusivities at 854 and 944 K. However, the shallow increase from zero to one benzene per supercage may not be statistically significant, given the relatively large error bars on these diffusivities.

In Figure 9A−C, we compare our simulated self-diffusion coefficients for benzene in NaX with the kinetic Monte Carlo (KMC) results of Saravanan and Auerbach,[15,50] and with experimental diffusivities from microscopic and macroscopic methods. In Figure 9A, the simulated diffusivities at 468 K are compared with PFG-NMR,[12] QENS,[49] frequency response (FR),[51] and tracer zero-length column (TZLC)[11] data. In Figure 9B, diffusivities at 403 K are compared with PFG-NMR[46,47] and QENS[49] measurements and in Figure 9C, diffusivities at 360 K are compared with PFG-NMR,[46] QENS,[49] and sorption uptake measurements (353 K).[47,52] The MD-simulated benzene self-diffusivities have been extrapolated to the temperatures of interest assuming an Arrhenius temperature dependence (as discussed earlier with reference to Figure 4). Our MD diffusivities are found to be in reasonably good agreement (within 1 order of magnitude) with PFG-NMR,[12,46,47] QENS,[49] and FR[51] data, while being significantly lower than Saravanan and

Auerbach's KMC estimations.[15,50] These KMC simulations involved a primitive treatment of guest−guest interactions, assuming that activation energies for site-to-site jumps could be estimated by nearest-neighbor bond-counting arguments. It is thus not surprising that the present MD simulations give results much closer to the truth. Inconsistent with all these, however, sorption uptake[47,52] and TZLC[11] experiments indicate a broadly increasing loading dependence. It remains to be discovered why these macroscopic methods show such different loading dependencies for benzene in NaX.[53]

IV. Summary and Concluding Remarks

We have revisited the problem of estimating benzene diffusivities in NaX through high-temperature molecular dynamics (MD) simulations. We re-optimized the guest−zeolite force field for use with our previously published explicit Si/Al framework model. We performed equilibrium molecular dynamics simulations at high temperatures and a wide range of loadings to simulate self-diffusion and Maxwell−Stefan diffusion of benzene in NaX. We found that Na cations remain largely immobile, even at elevated temperatures, lending credence to our approach of extrapolating high-temperature diffusivities to lower temperatures. The estimated temperature and loading dependencies of benzene self-diffusivities are in good agreement with PFG-NMR and QENS measurements. The MD-estimated self-diffusivities and Maxwell−Stefan diffusivities exhibit the Arrhenius temperature dependence, with activation energies in good agreement with available experimental data. Despite this agreement, we show in the following companion paper that membrane fluxes calculated with our diffusivities overestimate experiments by about 1 order of magnitude when support resistance effects are accounted for in the transport model, and by about 2 orders of magnitude when such resistances are neglected. This discrepancy may arise from the polycrystalline nature of present-day NaX membranes.

Acknowledgment. We gratefully acknowledge support from the Department of Energy (DE-FG02-94ER14485), the National Science Foundation (NSF CTS-0091406), and the National Environmental Technology Institute (NETI) for this project. We thank Dr. Cristian Blanco for expert assistance with the use of the Dizzy program. We also thank the reviewers for their comments and suggestions.

References and Notes

(1) Karger, J.; Vasenkov, S.; Auerbach, S. M. Diffusion in zeolites. In *Handbook of Zeolite Science and Technology*; Dutta, P. K., Ed.; Marcel-Dekker: New York, 2003; p 341.

(2) Karger, J.; Ruthven, D. *Diffusion in zeolites and other microporous solids*; Wiley: New York, 1992.

(3) Chen, N. Y.; Degnan, T. F.; Smith, C. M. *Molecular Transport and Reaction in Zeolites: Design and Application of Shape Selective Catalysts*; VCH: New York, 1994.

(4) Theodorou, D. N.; Snurr, R. Q.; Bell, A. T. Molecular dynamics and diffusion in microporous materials. In *Comprehensive Supramolecular Chemistry*; Bein, T., Ed.; Pergamon Press: Oxford, U.K., 1996; Vol. 7, p 507.

(5) Demontis, P.; Suffritti, G. B. *Chem. Rev.* **1997**, *97*, 2845.

(6) Keil, F. J.; Krishna, R.; Coppens, M. O. *Rev. Chem. Eng.* **2000**, *16*, 71.

(7) Auerbach, S. M. *Int. Rev. Phys. Chem.* **2000**, *19*, 155.

(8) Auerbach, S. M.; Jousse, F.; Vercauteren, D. P. Dynamics of Sorbed Molecules in Zeolites. In *Computer Modelling of Microporous and Mesoporous Materials*; Catlow, C. R. A., van Santen, R. A., Smit, B., Eds.; Elsevier: Amsterdam, 2004; p 49.

(9) *Modelling of Structure and Reactivity in Zeolites*; Catlow, C. R. A., Ed.; Academic Press: London, 1992; pp 260.

(10) Nair, S.; Tsapatsis, M. Synthesis and properties of zeolite membranes. In *Handbook of Zeolite Science and Technology*; Dutta, P. K., Ed.; Marcel-Dekker: New York, 2003; p 928.

(11) Brandani, S.; Xu, Z.; Ruthven, D. *Microporous Mater.* **1996**, *7*, 323.

(12) Germanus, A.; Karger, J.; Pfeifer, H.; Samulevic, N. N.; Zdanov, S. P. *Zeolites* **1985**, *5*, 91.

(13) Saravanan, C.; Jousse, F.; Auerbach, S. M. *J. Chem. Phys.* **1998**, *108*, 2162.

(14) Jousse, F.; Auerbach, S. M. *J. Chem. Phys.* **1997**, *107*, 9629.

(15) Saravanan, C.; Auerbach, S. M. *J. Chem. Phys.* **1999**, *110*, 11 000.

(16) Jaramillo, E.; Auerbach, S. M. *J. Phys. Chem. B* **1999**, *103*, 9589.

(17) Auerbach, S. M.; Henson, N. J.; Cheetham, A. K.; Metiu, H. I. *J. Phys. Chem.* **1995**, *99*, 10600.

(18) Auerbach, S. M.; Bull, L. M.; Henson, N. J.; Metiu, H. I.; Cheetham, A. K. *J. Phys. Chem.* **1996**, *100*, 5923.

(19) Vasenkov, S.; Galvosas, P.; Geier, O.; Nestle, N.; Stallmach, F.; Karger, J. *J. Magn. Reson.* **2001**, *149*, 228.

(20) Meier, W. M.; Olson, D. H.; Baerlocher, C. *Atlas of zeolite framework types*, 5th revised ed.; Elsevier: Amsterdam; New York, 2001.

(21) Catlow, C. R. A.; Freeman, C. M.; Vessal, B.; Tomlinson, S. M.; Leslie, M. *J. Chem. Soc., Faraday Trans.* **1991**, *87*, 1947.

(22) Turaga, S. C.; Auerbach, S. M. *J. Chem. Phys.* **2003**, *118*, 6512.

(23) Henson, N. J.; Auerbach, S. M.; Blanco, C. DIZZY Computational Chemistry Program, 1994 to present.

(24) Snyman, J. A. *Appl. Math. Modelling* **1982**, *6*, 449.

(25) Snyman, J. A. *Appl. Math. Modelling* **1983**, *7*, 216.

(26) Snyman, J. A. *Comput. Math. Appl.* **1989**, *17*, 1369.

(27) Fitch, A. N.; Jobic, H.; Renouprez, A. *J. Phys. Chem.* **1986**, *90*, 1311.

(28) Vitale, G.; Mellot, C. F.; Bull, L. M.; Cheetham, A. K. *J. Phys. Chem. B* **1997**, *101*, 4559.

(29) Allen, M. P.; Tildesley, D. J. *Computer simulation of liquids*; Clarendon Press: Oxford University Press: Oxford [Oxfordshire], New York, 1987.

(30) Mortier, W. J.; Schoonheydt, R. A. *Prog. Solid State Chem.* **1985**, *16*, 1.

(31) Jansen, F. J.; Schoonheydt, R. A. *J. Chem. Soc., Faraday Trans. I* **1973**, *69*, 1338.

(32) Hunger, M.; Buchholz, A.; Schenk, U. High-temperature MAS NMR investigation of the mobility of cations and guest compounds in zeoilites X and Y; 13th International Zeolite Conference, 2001, Montpellier, France.

(33) Barrer, R. M.; Rees, L. V. C. *Trans. Faraday Soc.* **1960**, *56*, 709.

(34) Feuerstein, M.; Lobo, R. F. *Solid State Ionics* **1999**, *118*, 135.

(35) Paschek, D.; Krishna, R. *Phys. Chem. Chem. Phys.* **2000**, *2*, 2389.

(36) Krishna, R.; Paschek, D. *Chem. Eng. J.* **2002**, *87*, 1.

(37) Maginn, E. J.; Bell, A. T.; Theodorou, D. N. *J. Phys. Chem.* **1993**, *97*, 4173.

(38) Sanborn, M. J.; Snurr, R. Q. *AIChE J.* **2001**, *47*, 2032.

(39) Skoulidas, A. I.; Sholl, D. S. *J. Phys. Chem. A* **2003**, *107*, 10132.

(40) www.statpages.net. Least-squares fitting program with error in X and Y.

(41) Chen, L. G.; Falcioni, M.; Deem, M. W. *J. Phys. Chem. B* **2000**, *104*, 6033.

(42) Dzhigit, O. M.; Kiselev, A. V.; Rachmanova, T. A. *Zeolites* **1984**, *4*, 389.

(43) Olson, D. H. *Zeolites* **1995**, *15*, 439.

(44) Buttefey, S.; Boutin, A.; Mellot-Draznieks, C.; Fuchs, A. H. *J. Phys. Chem. B* **2001**, *105*, 9569.

(45) Karger, J.; Caro, J. *J. Chem. Soc., Faraday Trans. I* **1977**, *73*, 1363.

(46) Lorenz, P.; Bulow, M.; Karger, J. *Izv. Akad. Nauk SSSR, Ser. Khim.* **1980**, 1741.

(47) Karger, J.; Ruthven, D. M. *J. Chem. Soc., Faraday Trans. I* **1981**, *77*, 1485.

(48) Jobic, H.; Bee, M.; Karger, J.; Pfeifer, H.; Caro, J. *J. Chem. Soc., Chem. Commun.* **1990**, 341.

(49) Jobic, H.; Fitch, A. N.; Combet, J. *J. Phys. Chem. B* **2000**, *104*, 8491.

(50) Saravanan, C.; Jousse, F.; Auerbach, S. M. *Phys. Rev. Lett.* **1998**, *80*, 5754.

(51) Shen, D. M.; Rees, L. V. C. *Zeolites* **1991**, *11*, 666.

(52) Bulow, M.; Struve, P.; Mietk, W. *J. Chem. Soc., Faraday Trans. I* **1984**, *80*, 813.

(53) Vasenkov, S.; Bohlmann, W.; Galvosas, P.; Geier, O.; Liu, H.; Karger, J. *J. Phys. Chem. B* **2001**, *105*, 5922.

(54) Barthomeuf, D.; Ha, B. H. *J. Chem. Soc., Faraday Trans. I* **1973**, *69*, 2147.

(55) Barthomeuf, D.; Ha, B. H. *J. Chem. Soc., Faraday Trans. I* **1973**, *69*, 2158.